

Dalton Transactions

Accepted Manuscript



This is an *Accepted Manuscript*, which has been through the Royal Society of Chemistry peer review process and has been accepted for publication.

Accepted Manuscripts are published online shortly after acceptance, before technical editing, formatting and proof reading. Using this free service, authors can make their results available to the community, in citable form, before we publish the edited article. We will replace this *Accepted Manuscript* with the edited and formatted *Advance Article* as soon as it is available.

You can find more information about *Accepted Manuscripts* in the [Information for Authors](#).

Please note that technical editing may introduce minor changes to the text and/or graphics, which may alter content. The journal's standard [Terms & Conditions](#) and the [Ethical guidelines](#) still apply. In no event shall the Royal Society of Chemistry be held responsible for any errors or omissions in this *Accepted Manuscript* or any consequences arising from the use of any information it contains.

New Insight into the Chemistry of Iridium(III) Complexes Bearing Phenyl Phenylphosphonite Cyclometalate and Chelating Pyridyl Triazolate: The Excited-State Proton Transfer Tautomerism via Inter-ligand PO-H...N Hydrogen Bond

Cheng-Huei Lin,^a Jia-Ling Liao,^a Yu-Sin Wu,^b Kuan-Yu Liao,^a Yun Chi,^{*,a,c} Chi-Lin Chen,^b Gene-Hsiang Lee^b and Pi-Tai Chou^{*,b,d}

^a Department of Chemistry, National Tsing Hua University, Hsinchu 30013, Taiwan; E-mail: ychi@mx.nthu.edu.tw

^b Department of Chemistry, National Taiwan University, Taipei 10617, Taiwan; E-mail: chop@ntu.edu.tw

^c Low Carbon Energy Research Center, National Tsing Hua University, Hsinchu 30013, Taiwan

^d Center for Emerging Material and Advanced Devices, National Taiwan University, Taipei 10617, Taiwan

KEYWORDS. *Hydrogen Bonding, Excited State Proton Transfer, Iridium Complexes, Phosphorescence, Proton Transfer Tautomerism*

Received (in XXX, XXX) Xth XXXXXXXXX 20XX, Accepted Xth XXXXXXXXX 20XX

DOI: 10.1039/b000000x

ABSTRACT: Treatment of $[\text{IrCl}_3(\text{tht})_3]$, tht = tetrahydrothiophene, with two equiv. of phenyl diphenylphosphinite (pdpitH) gave $[\text{Ir}(\text{pdpitH})(\text{pdpit})(\text{tht})\text{Cl}_2]$ (**1**), for which further reaction with 3-*t*-butyl-5-(2-pyridyl)-1,2,4-triazole (bptzH) and NaOAc using an one-pot reaction afforded $[\text{Ir}(\text{pdpit})_2(\text{bptz})]$ (**2**). In sharp contrast, the reaction of $[\text{IrCl}_3(\text{tht})_3]$, pdpitH, bptzH and in presence of a stronger base Na_2CO_3 afforded a phenyl phenylphosphonite (pppo)-containing Ir(III) complex $[\text{Ir}(\text{pdpit})(\text{pppo})(\text{bptz})]$ (**3**) that reveals a strong PO-H-N inter-ligand hydrogen bond (H-bond), as evidenced by the single crystal X-ray structural analysis. For confirmation, addition of diazomethane to a diethylether solution of **3** gave isolation of two methylated Ir(III) isomeric complexes, i.e. $[\text{Ir}(\text{pdpit})(\text{pppoMe})(\text{bptz})]$ (**4**) and $[\text{Ir}(\text{pdpit})(\text{pppo})(\text{bptzMe})]$ (**5**) possessing either PO-Me or N-Me bonding fragment, respectively. The absorption spectrum of **3** in CH_2Cl_2 resembles that of **4**, implying the dominant PO-H character in solution. Despite the prevailing PO-H character in both solid crystal and solution, its corresponding emission resembles that of **5**, leading us to propose a mechanism incorporating excited-state inter-ligand proton transfer (ESILPT) from PO-H to N-H isomeric form via the pre-existing PO...H...N hydrogen bond. Thermodynamics of proton transfer tautomerism are discussed under the basis of absorption/emission spectroscopy in combination with computational approaches; additional support is given by the relationship between emission pattern versus the position of proton and methyl substituent. The results demonstrate for the first time a paradigm of excited-state proton transfer for the transition metal complexes in the triplet manifold.

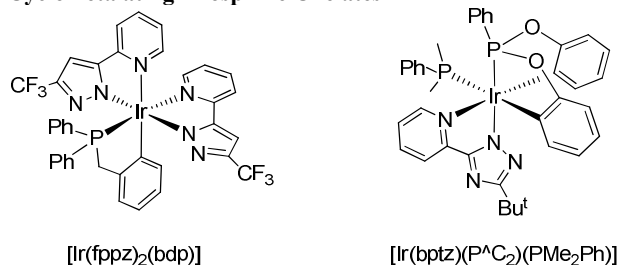
Introduction

Proton transfer is considered to be one of the most fundamental processes involved in chemical and biochemical reactions. Among various proton transfer systems, those invoking excited state proton transfer (ESPT) have received much attention.^{1, 2} At the molecular level, ESPT involves transfer of protons from the donor (D) to either the solvent molecules or to the proton acceptor (A) in the electronically excited state, the prerequisite of which requires unique arrangement/relay of the hydrogen bonds.³ The latter case involves proton transfer within the same molecule or self-dimer and D/A complex via hydrogen-bond (H-bond) formation such that ESPT takes place between proton donating and accepting molecules along the H-bond.⁴⁻¹¹ This reaction pattern is commonly dubbed as excited-state intramolecular proton transfer (ESIPT), which occurs in an unimolecular basis with pre-existing intramolecular H-bonds between proton donor and acceptor.⁸ ESIPT has long been served as a model to mimic and gain insight into e.g., catalytic and biocatalytic reactions.¹²⁻¹⁷

Of equal importance are their realization and perspective in emerging optoelectronic applications.^{4, 5, 7} To this contribution, our recent focus was on the relationship for the ESPT dynamics versus H-bond strength and geometry^{6, 11} as well as ESPT application toward white light generation.⁵ In yet another research direction focused on highly emissive transition metal complexes, we have accomplished studies on the assembly of various true-blue and blue phosphors using a class of higher $\pi\pi^*$ energy-gap pyridyl azolate chromophores, together with the cyclometalating phosphine ancillaries such as bi-dentate benzyldiphenylphosphine¹⁸ or tripodal coordinated phenyl diphenylphosphinite.^{19, 20} Representative molecular structures are depicted below, which exhibit bright phosphorescence in both solid and doped films at room temperature (RT), paving a new way for designing blue-emitting phosphors without the employment of 4,6-difluorophenylpyridinato chelate in FIrpic and analogues, as the ortho-fluorine substituent is known to be exceedingly labile at elevated temperature, especially during practical device operation,²¹ giving inferior lifespan for the as-fabricated true-blue and blue OLEDs.²²

Combining ample experiences in both fields, we have long been searching for ESIPT in the transition metal complex. This research underscores several important issues, namely: (i) The enhanced spin-orbit coupling may lead to the occurrence of ESIPT in both singlet and triplet manifolds; the latter is otherwise obscure in most organic ESIPT systems. (ii) Since the transition metal complex is composed of various ancillary chromophores, a

Chart 1. Blue-emitting Ir(III) complexes with Cyclometalating Phosphine Chelates



case of ESIPT through inter-ligand H-bond would be unprecedented and hence of great fundamental interest. (iii) As for Ir(III) or Ru(II) complexes ubiquitously applied in the OLEDs, solar cells and photo-catalysis,²³ the electronic transition normally involves a hybrid of ligand-centered $\pi\pi^*$ and MLCT (metal to ligand charge transfer). The occurrence of ESIPT thus pumps the metal d-electron toward proton-transfer isomerization, which may drastically alter the excited-state properties, for example the photo-catalytic effect.

Attaining ESIPT for the transition metal complexes requires a strategic design of the transition metal complex endowed with either intra-ligand or inter-ligand H-bonding formation. In this contribution, we reported on the stepwise steps transformation among Ir(III) complexes that are synthesized with employment of phenyl diphenylphosphinite (pdpitH) ancillary. In sharp contrast to the simple cyclometalation observed for analogous benzyldiphenylphosphine,²⁴⁻²⁸ the pdpitH molecule has displayed an additional reaction pattern upon switching the cyclometalation catalyst from NaOAc to the much basic Na₂CO₃, that is, the temporal formation of species equivalent to diphenyl phenylphosphonite (i.e. concomitant metathesis of aryl substituents), followed by cleavage of one phenyl-oxygen bonding, giving a coordinated phenyl phenylphosphonite (pppo) fragment. Moreover, this pppo ligand reveals an interligand H-bonding to the adjacent nitrogen atom of the pyridyl triazolate chromophore. It is thus of great fundamental interest to gain in-depth insight into how this interligand H-bonding would affect the corresponding chemical properties as well as the associated photophysical phenomena. As a result, we report for the first time the excited-state inter-ligand proton transfer within the framework of phosphorescent transition-metal complexes, adding a new dimension to the field of the excited-state proton transfer process^{1, 29, 30} that overwhelmingly takes place in the fluorescent organic molecules. Detail of our investigation is elaborated in the following sections.

Experimental

45 General procedures.

All reactions were performed under argon atmosphere and solvents were distilled from appropriate drying agents prior to use. Commercially available reagents were used without further purification unless otherwise stated. All reactions were monitored using pre-coated TLC plates (0.20 mm with fluorescent indicator UV254). Mass spectra were obtained with a JEOL SX-102A instrument operating in electron impact (EI) or fast atom bombardment (FAB) mode. ¹H and ³¹P NMR spectra were recorded on a Varian Mercury-400 or an INOVA-500 instrument. Elemental analysis was carried out with a Heraeus CHN-O Rapid Elemental Analyzer. The phosphorous donor ligands, phenyl diphenylphosphinite (pdpitH) and diphenyl phenylphosphonite (dppon) were synthesized according to the literature methods.³¹ An ethereal solution of diazomethane was prepared from DiazaldTM and KOH in a mixture of carbitol, water and diethylether.³² **Caution:** diazomethane is extremely toxic and potentially explosive. Hazard is reduced by conducting reaction in glassware equipped with clear glass joints and always using the diluted diazomethane solution.

Preparation of [Ir(pdpiH)(pdpit)(tht)Cl₂] (**1**): A mixture of IrCl₃(tht)₃ (200 mg, 0.36 mmol) and phenyl diphenylphosphinite (pdpitH, 307 mg, 1.10 mmol) in decalin (12 mL) was heated to reflux for 24 hr. After cooling to RT, the solvent was removed under vacuum and the residue was washed with CH₂Cl₂ and ether to give white powder (228 mg, 0.25 mmol, 70.8%). Single crystals of **1** were obtained from a mixture of CH₂Cl₂ and methanol at RT.

Spectral data of **1**: MS (FAB, ¹⁹³Ir): *m/z* 872 (M-Cl)⁺; ¹H NMR (500 MHz, CD₂Cl₂, 233 K): δ 8.21 (br, 2H), 7.66 (t, *J* = 9.0 Hz, 2H), 7.58 ~ 7.51 (m, 3H), 7.51 ~ 7.43 (m, 2H), 7.39 ~ 7.28 (m, 8H), 7.19 (d, *J* = 7.5 Hz, 1H), 7.15 (t, *J* = 7.5 Hz, 1H), 7.07 (t, *J* = 7.5 Hz, 1H), 6.89 (br, 2H), 6.80 (t, *J* = 7.5 Hz, 2H), 6.73 (t, *J* = 7.5 Hz, 1H), 6.67 (t, *J* = 7.5 Hz, 1H), 6.47 (br, 1H), 6.18 (d, *J* = 7.5 Hz, 2H), 3.86 (m, 1H), 2.82 (m, 1H), 2.10 (m, 1H), 1.89 (m, 1H), 1.79 (m, 1H), 1.68 ~ 1.60 (m, 2H), 1.54 (m, 1H). ³¹P-{¹H} NMR (202 MHz, CDCl₃, 294 K): δ 91.16 (d, *J*_{PP} = 23.2 Hz, 1P), 70.55 (d, *J*_{PP} = 23.2 Hz, 1P). Anal. Calcd. for C₄₀H₃₇Cl₂IrO₂P₂S: C, 52.98; H, 4.11. Found: C, 52.44; H, 4.20.

Selected crystal data of **1**: C₄₁H₃₉C₁₄IrO₂P₂S; M = 991.72; monoclinic; space group = P₂₁/n; a = 9.0297(5) Å, b = 10.6379(6) Å, c = 40.142(2) Å, β = 92.521(2)°; V = 3852.2(4) Å³; Z = 4; ρ_{calcd} = 1.710 Mg·m⁻³; F(000) = 1968; crystal size = 0.40 × 0.15 × 0.10 mm³; $\lambda(\text{Mo-K}\alpha)$ = 0.71073 Å; T = 150(2) K; μ = 3.917 mm⁻¹; 27821 reflections collected, 8768 independent reflections (*R*_{int} = 0.0412), GOF = 1.134, final *R*₁[*I* > 2 σ (*I*)] = 0.0359 and *wR*₂(all data) = 0.0732.

Preparation of [Ir(pdpiH)₂(bptz)] (**2**): IrCl₃(tht)₃ (200 mg, 0.36 mmol), pdpitH (210 mg, 0.78 mmol) were combined in decalin (12 mL) and the mixture was heated at 190°C for 3 hr. After cooling to RT, 3-*t*-butyl-5-(2-pyridyl)-1,2,4-triazole (bptzH, 79 mg, 0.39 mmol) and sodium acetate (NaOAc, 291 mg, 3.56 mmol) were added and the mixture was heated at 196°C for another 13 hr. Finally, the solvent was removed and the residue was purified by silica gel column chromatography using a 2:1 mixture of ethyl acetate and hexane as the eluent. The pale green crystals of [Ir(pdpiH)₂(bptz)] were obtained by slow diffusion of hexane into a CH₂Cl₂ solution at RT (134 mg, 0.14 mmol, 39.8%).

Single crystals of **2** were obtained from a mixture of CH₂Cl₂ and hexane at RT.

Spectra data of **2**: MS (FAB, ¹⁹³Ir): *m/z* 948 (M⁺); ¹H NMR (400 MHz, CDCl₃, 298 K): 7.94 ~ 7.82 (m, 5H), 7.56 ~ 7.46 (m, 2H), 7.42 (t, *J* = 7.2 Hz, 1H), 7.37 (t, *J* = 7.2 Hz, 1H), 7.32 ~ 7.21 (m, 4H), 7.12 ~ 7.06 (m, 2H), 6.97 (t, *J* = 7.6 Hz, 1H), 6.94 ~ 6.76 (m, 6H), 6.72 (d, *J* = 7.6 Hz, 1H), 6.69 ~ 6.61 (m, 3H), 6.58 (t, *J* = 7.2 Hz, 1H), 6.54 ~ 6.47 (m, 2H), 6.33 (t, *J* = 8.8 Hz, 2H), 5.84 (t, *J* = 6.2 Hz, 1H), 1.42 (s, 9H). ³¹P-¹H NMR (202 MHz, CDCl₃, 298 K): δ 106.70 (d, *J*_{PP} = 6.4 Hz 1P), 102.27 (d, *J*_{PP} = 6.4 Hz, 1P). Anal. calcd. for C₄₇H₄₁IrN₄O₂P₂: N, 5.91; C, 59.55; H, 4.36. Found: N, 5.99; C, 58.95; H, 4.47.

Selected crystal data of **2**: C₄₇H₄₁IrN₄O₂P₂; M = 947.98; orthorhombic; space group = *Pbca*; *a* = 14.7866(7) Å, *b* = 17.6171(8) Å, *c* = 30.5710(15) Å, *V* = 7963.7(7) Å³; *Z* = 4; ρ_{calcd} = 1.581 Mg·m⁻³; *F*(000) = 3792; crystal size = 0.50 × 0.43 × 0.28 mm³; λ(Mo-K_α) = 0.71073 Å; *T* = 150(2) K; μ = 3.479 mm⁻¹; 42086 reflections collected, 9143 independent reflections (*R*_{int} = 0.0426), *GOF* = 1.119, final *R*₁[*I* > 2σ(*I*)] = 0.0267 and *wR*₂(all data) = 0.0732.

Preparation of [Ir(pdpt)(pppo)(bptz)] (**3**): IrCl₃(tht)₃ (202 mg, 0.36 mmol), pdptH (210 mg, 0.78 mmol) were combined in decalin (12 mL) and the mixture was heated at 190°C for 5 hr. After cooling to RT, bptzH (76 mg, 0.38 mmol) and Na₂CO₃ (188 mg, 1.77 mmol) were added and the mixture was heated at 196°C for another 13 hr. Finally, the solvent was removed and the residue was purified by silica gel column chromatography using a 1:1 mixture of ethyl acetate and hexane as the eluent. The green crystals of [Ir(pdpt)(pppo)(bptz)] (**3**) were obtained by slow diffusion of methanol into a CH₂Cl₂ solution at RT (150 mg, 0.169 mmol, 47.0%). Single crystals of **3** were obtained from a mixture of CH₂Cl₂ and hexane at RT.

Method 2: Complex **1** (178 mg, 0.20 mmol), diphenyl phenylphosphonite (dppon, 63 mg, 0.214 mmol), Na₂CO₃ (104 mg, 0.98 mmol) and bptzH (43 mg, 0.21 mmol) were combined in decalin (8 mL) and the mixture was heated at 180°C for 12 hour. After chromatographic separation and recrystallization, complex **3** was obtained in 17.8% yield (31 mg, 0.03 mmol).

Spectra data of **3**: MS (FAB, ¹⁹³Ir): *m/z* 888 (M+1)⁺; ¹H NMR (400 MHz, 1.35 × 10⁻⁴ M in CDCl₃, 298 K): δ 12.42 (s, br, 1H), 7.96 (d, *J* = 8.4 Hz, 1H), 7.71 (br, 1H), 7.63 (t, *J* = 7.8 Hz, 1H), 7.44 ~ 7.35 (m, 3H), 7.34 ~ 7.27 (m, 2H), 7.15 (t, *J* = 7.6 Hz, 1H), 7.05 ~ 6.88 (m, 5H), 6.86 ~ 6.77 (m, 5H), 6.69 ~ 6.52 (m, 5H), 6.50 ~ 6.41 (m, 2H), 6.01 (t, *J* = 6.4 Hz, 1H), 4.61 (br, 1H, OH), 1.54 (s, 9H). ³¹P-¹H NMR (202 MHz, CDCl₃, 298 K): δ 106.16 (d, *J*_{PP} = 10.2 Hz, 1P), 94.11 (d, *J*_{PP} = 10.2 Hz 1P). Anal. calcd. for C₄₁H₃₇IrN₄O₃P₂: N, 6.31; C, 55.46; H, 4.20. Found: N, 6.37; C, 54.99; H, 4.45.

Selected crystal data of **3**: C₄₂H_{39.4}Cl_{2.4}IrN₄O₃P₂; M = 990.31; monoclinic; space group = *P2₁/n*; *a* = 13.2294(6) Å, *b* = 22.1241(10) Å, *c* = 14.3469(7) Å, β = 98.5169(10)°, *V* = 4152.9(3) Å³; *Z* = 4; ρ_{calcd} = 1.584 Mg·m⁻³; *F*(000) = 1971; crystal size = 0.25 × 0.20 × 0.10 mm³; λ(Mo-K_α) = 0.71073 Å; *T* = 150(2) K; μ = 3.529 mm⁻¹; 31860 reflections collected, 9538 independent reflections (*R*_{int} = 0.0472), *GOF* = 1.056, final *R*₁[*I* > 2σ(*I*)] = 0.0437 and *wR*₂(all data) = 0.1079.

Methylation of **3**: The diazomethane etherate in excess was added to a solution of **3** (700 mg, 0.79 mmol) in ether (150 mL) at 0°C. After the completion of addition, the mixture was stirred for 4 hr at RT, the solvent was removed, and the residue was purified by silica gel column chromatography using a 1:2 mixture

of ethyl acetate and hexane as the eluent, affording a light yellow and a pale green band in an approx. 2:1 ratio. The yellow crystals of [Ir(pdpt)(pppoMe)(bptz)] (**4**) (407 mg, 0.45 mmol, 57.2%) and pale green crystals of [Ir(pdpt)(pppo)(bptzMe)] (**5**) (204 mg, 0.23 mmol, 28.7%) were next obtained by slow diffusion of hexane into an acetone solution of complex, and from the mixture of CH₂Cl₂ and hexane at RT, respectively.

Spectra data of **4**: MS (FAB, ¹⁹³Ir): *m/z* 902 (M⁺); ¹H NMR (400 MHz, CD₂Cl₂, 298 K): δ 8.21 ~ 8.13 (m, 2H), 7.69 (d, *J* = 8.0 Hz, 1H), 7.63 ~ 7.49 (m, 5H), 7.17 ~ 7.09 (m, 2H), 7.04 (t, *J* = 7.2 Hz, 1H), 6.99 ~ 6.91 (m, 2H), 6.84 (td, *J* = 7.6, 2.4 Hz, 2H), 6.81 ~ 6.71 (m, 4H), 6.71 ~ 6.62 (m, 2H), 6.56 (dd, *J* = 7.6, 1.6 Hz, 1H), 6.37 ~ 6.29 (m, 2H), 6.27 ~ 6.19 (m, 2H), 6.00 (t, *J* = 6.5 Hz, 1H), 4.01 (d, *J*_{PH} = 12.0 Hz, 3H), 1.51 (s, 9H). ³¹P-¹H NMR (202 MHz, CD₂Cl₂, 298 K): δ 117.55 (d, *J*_{PP} = 12.3 Hz, 1P), 108.21 (d, *J*_{PP} = 12.3 Hz, 1P). Anal. calcd. for C₄₂H₃₉IrN₄O₃P₂: N, 6.21; C, 55.93; H, 4.36. Found: N, 5.84; C, 56.33; H, 5.05.

Selected crystal data of **4**: C₄₈H₅₃IrN₄O₃P₂; M = 988.08; monoclinic; space group = *P2₁/c*; *a* = 15.0395(6) Å, *b* = 20.7656(9) Å, *c* = 14.4577(6) Å, β = 99.8210(9)°, *V* = 4449.0(3) Å³; *Z* = 4; ρ_{calcd} = 1.475 Mg·m⁻³; *F*(000) = 2000; crystal size = 0.50 × 0.25 × 0.20 mm³; λ(Mo-K_α) = 0.71073 Å; *T* = 150(2) K; μ = 3.118 mm⁻¹; 32724 reflections collected, 10235 independent reflections (*R*_{int} = 0.0404), *GOF* = 1.149, final *R*₁[*I* > 2σ(*I*)] = 0.0345 and *wR*₂(all data) = 0.0979.

Spectra data of **5**: MS (FAB, ¹⁹³Ir): *m/z* 903 (M+1)⁺; ¹H NMR (400 MHz, d₆-acetone, 298 K): δ 8.14 ~ 8.02 (m, 2H), 7.95 ~ 7.82 (m, 2H), 7.64 ~ 7.53 (m, 3H), 7.44 (br, 1H), 7.14 (t, *J* = 6.6 Hz, 1H), 6.99 (t, *J* = 7.2 Hz, 1H), 6.95 ~ 6.84 (m, 5H), 6.78 (t, *J* = 7.2 Hz, 1H), 6.66 ~ 6.53 (m, 6H), 6.52 ~ 6.41 (m, 4H), 5.90 (t, *J* = 6.4 Hz, 1H), 5.09 (s, 3H), 1.56 (s, 9H). ³¹P-¹H NMR (202 MHz, d₆-acetone, 298 K): δ 114.01 (d, *J*_{PP} = 14.0 Hz, 1P), 64.34 (d, *J*_{PP} = 14.0 Hz, 1P). Anal. calcd. for C₄₂H₃₉IrN₄O₃P₂: N, 6.21; C, 55.93; H, 4.36. Found: N, 6.37; C, 55.82; H, 4.47.

Selected crystal data of **5**: C₄₃H₄₁Cl₂IrN₄O₃P₂; M = 986.84; monoclinic; space group = *P2₁/c*; *a* = 11.6481(5) Å, *b* = 21.5974(10) Å, *c* = 16.3516(7) Å, β = 101.4744(11)°, *V* = 4031.3 Å³; *Z* = 4; ρ_{calcd} = 1.626 Mg·m⁻³; *F*(000) = 1968; crystal size = 0.25 × 0.13 × 0.10 mm³; λ(Mo-K_α) = 0.71073 Å; *T* = 150(2) K; μ = 3.569 mm⁻¹; 30935 reflections collected, 9249 independent reflections (*R*_{int} = 0.0733), *GOF* = 1.012, final *R*₁[*I* > 2σ(*I*)] = 0.0399 and *wR*₂(all data) = 0.0816.

Preparation of **6**: A 10 mL THF solution of **3** (71 mg, 0.08 mmol) was transferred in a reaction flask containing NaH (3 mg, 0.12 mmol). The mixture was stirred for 2 h at RT until the gas evolution ceased. The solution was filtered through a pad of Celite and the filtrate was concentrated to dryness, giving a pale green powder of Na[Ir(pdpt)(pppo)(bptz)] (**6**) (50 mg, 0.027 mmol, 67%). Single crystals of **6** suitable for X-ray analysis were obtained from a mixture of CH₂Cl₂ and MeOH at RT.

Spectra data of **6**: ¹H NMR (400 MHz, CD₂Cl₂, 298 K): δ 7.93 (d, 1H, *J* = 8.0 Hz), 7.91 (d, 1H, *J* = 8.4 Hz), 7.66 (d, 1H, *J* = 7.8 Hz), 7.54 ~ 7.48 (m, 5H), 7.05 (t, 3H, *J* = 6.5 Hz), 6.90 ~ 6.82 (m, 2H), 6.79 ~ 6.70 (m, 6H), 6.62 (d, 1H, *J* = 7.8 Hz), 6.58 ~ 6.56 (m, 3H), 6.31 (t, 4H, *J* = 7.8 Hz), 6.00 (t, 1H, *J* = 5.7 Hz), 3.30 (s, MeOH, 3H), 1.00 (s, 9H). ³¹P-¹H NMR (202 MHz, CD₂Cl₂, 298 K): δ 109.14 (d, *J*_{PP} = 14.1 Hz, 1P), 84.14 (d, *J*_{PP} = 13.0 Hz, 1P).

Selected crystal data of **6**: C₈₆H₈₈Ir₂N₈Na₂O₁₀P₄; M = 1947.90; triclinic; space group = *P-1*; *a* = 12.3478(10) Å, *b* = 12.8587(11) Å, *c* = 15.8042(13) Å, α = 96.292(2)°, β = 109.712(2)°, γ =

114.102(2)°, $V = 2065.1(3) \text{ \AA}^3$; $Z = 1$; $\rho_{\text{calcd}} = 1.566 \text{ Mg}\cdot\text{m}^{-3}$; $F(000) = 976$; crystal size = $0.25 \times 0.16 \times 0.13 \text{ mm}^3$; $\lambda(\text{Mo-K}\alpha) = 0.71073 \text{ \AA}$; $T = 150(2) \text{ K}$; $\mu = 3.370 \text{ mm}^{-1}$; 24667 reflections collected, 9422 independent reflections ($R_{\text{int}} = 0.0505$), $\text{GOF} = 1.010$, final $R_1[I > 2\sigma(I)] = 0.0345$ and $wR_2(\text{all data}) = 0.0699$.

Single Crystal X-Ray Diffraction Studies. Single crystal X-ray diffraction data were measured on a Bruker SMART Apex CCD diffractometer using Mo radiation ($\lambda = 0.71073 \text{ \AA}$). The data collection was executed using the SMART program. Cell refinement and data reduction were performed with the SAINT program. An empirical absorption was applied based on the symmetry-equivalent reflections and the SADABS program. The structures were solved using the SHELXS-97 program and refined using SHELXL-97 program by full-matrix least squares on F^2 values. The structural analysis and molecular graphics were obtained using SHELXTL program on PC computer.³³ All hydrogen atoms attached to the carbon atoms were fixed at calculated positions and refined using a riding mode. The hydrogen atom H(2) of Pt(II) complex 3 was located in a difference Fourier map; its atomic coordinates were then refined and with the Uiso fixed to 1.5 Ueq of its parent O(2) atom. CCDC 1025244 - 1025249 contain the supplementary crystallographic data for this paper. These data can be obtained free of charge from the Cambridge Crystallographic Data Centre via [www.ccdc.cam.ac.uk/data request/cif](http://www.ccdc.cam.ac.uk/data_request/cif).

Photophysical Measurement.

Steady-state absorption and emission spectra were recorded with a Hitachi (U-3310) spectrophotometer and an Edinburgh (FS920) fluorimeter, respectively. Both wavelength-dependent excitation and emission response of the fluorimeter have been calibrated. The various solvents were of spectrally grade quality (Merck Inc.) and were used as received. To determine the photoluminescence quantum yield in solution, samples were degassed by three freeze-pump-thaw cycles. Coumarin 480 in methanol with an emission yield of $\Phi \sim 0.87$ was used as reference to determine quantum yields for the studied compounds in solution. Lifetime studies were performed by an Edinburgh FL 900 time correlated single photon counting (TCSPC) system with a hydrogen-filled lamp as the excitation source. Data were analyzed using the nonlinear least squares procedure in combination with an iterative convolution method. Single-exponential emission decay was obtained for all studied compounds.

Nanosecond transient absorption was recorded with a laser photolysis system, in which the third harmonic (355 nm) of a Nd:YAG laser (Continuum Surelite) was used as the pump pulse. The Nd:YAG pump pulse was fired at a 1 Hz repetition rate and synchronized with a white light (xenon arc lamp) pulse acting as the probe beams. Two pulses were crossed at a 90° angle with an overlapping distance of 10 mm. The temporal resolution was limited by an excitation pulse duration of approximately 10 ns.

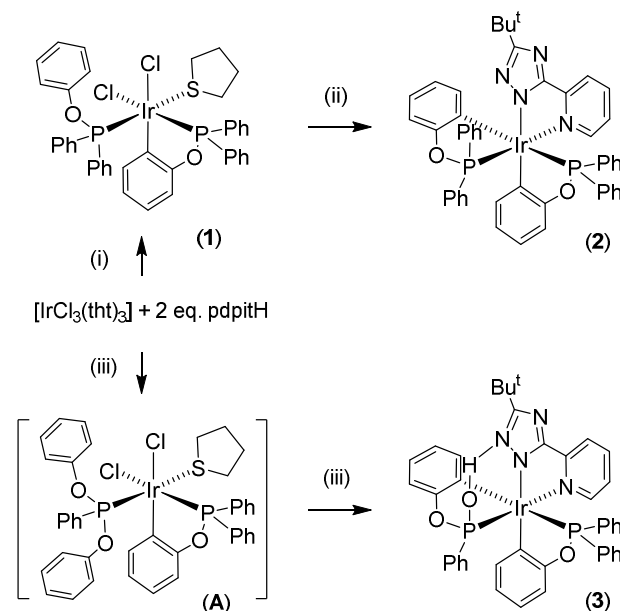
The femtosecond UV/vis transient absorption measurements were also performed according to the previous reports.³⁴ Briefly, femtosecond Ti:sapphire amplifier was used as the light source. The output of the system consists of pulses of 800 nm, 1 W, 220 fs (fwhm) at a repetition rate of 1 kHz. The laser amplifier output is first split half into two beams, in which the pump is converted to 400 nm by coupling it into a second-harmonic generator. The probe 800 nm is focused on a 1 mm thick sapphire plate to generate a white light continuum. The pump beam is then passed through an optical chopper and focused on a 1 mm optical path quartz disc-shape cell placed in a variable speed rotating holder. The white continuum after passing through the sample cell is

coupled into a 100 μm optical fiber connected to a diode array. The time-resolved absorption spectra were acquired via an average of 300 excitation pulses at each pump-probe delay time.

Computational methodology.

Calculations on electronic singlet and triplet states of all titled complexes were carried out using the density functional theory (DFT) with B3LYP hybrid functional.^{35, 36} Restricted and unrestricted formalisms were adopted in the singlet and triplet geometry optimization, respectively. A “double- ζ ” quality basis set consisting of Hay and Wadt's effective core potentials (LANL2DZ)^{37, 38} was employed for the Ir(III) metal atom, and a 6-31G* basis set,³⁹ for the rest of atoms. The relativistic effective core potential (ECP) replaced the inner core electrons of Ir(III) metal atom, leaving only the outer core valence electrons ($5s^2 5p^6 5d^6$) to be concerned. Time-dependent DFT (TDDFT) calculations using the B3LYP functional were then performed based on the optimized structures at the ground state.⁴⁰⁻⁴⁴

Scheme 1. Synthetic protocols to the studied Ir(III) complexes; reagents and experimental conditions.^a



^a(i) decalin, reflux, 24 h, (ii) bptzH, NaOAc, decalin, 196°C, 13 h, (iii) bptzH, Na₂CO₃, decalin, 196°C, 13 h.

Considering the solvation effect, the calculations were then combined with a polarizable conductor continuum model CPCM (in dichloromethane) implemented in Gaussian 09.⁴⁵ Typically, 10 lower triplet and singlet roots of the non-hermitian eigenvalue equations were obtained to determine the vertical excitation energies. Oscillator strengths were then deduced from the dipole transition matrix elements (for singlet states only). All calculations were carried out using Gaussian 09.⁴⁶

Result and discussion

Synthesis and characterization

Treatment of Ir(III) source complex $[\text{Ir}(\text{tht})_3\text{Cl}_3]$ with two equivalent of phenyl diphenylphosphinite (pdpitH) in refluxing decalin for an extended period of time afforded the di-substitution product $[\text{Ir}(\text{pdpitH})(\text{pdpit})(\text{tht})\text{Cl}_2]$ (1) in excellent yield, for which the spectroscopic and mass analysis showed retention of one tht ligand and attachment of two diphenylphosphinite units;

the latter is also confirmed by the observation of two ^{31}P NMR signals with equal intensity at δ 91.16 and 70.55. Subsequently, treatment of **1** with 3-*t*-butyl-5-(2-pyridyl)-1,2,4-triazole (bptzH) in presence of sodium acetate (NaOAc) as both the HCl scavenger and cyclometalation promoter, or using the *in-situ* synthesized **1** as the metal source, led to the isolation of a weakly emissive $[\text{Ir}(\text{pdpit})_2(\text{bptz})]$ (**2**) in moderate yield (Scheme 1). This synthetic pattern is analogous to that of the

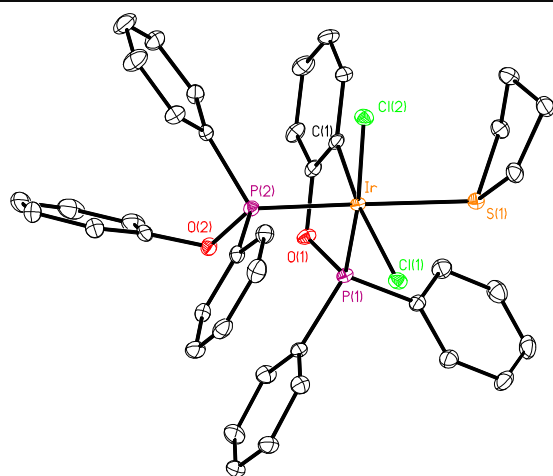


Figure 1. Structural drawing of **1** with ellipsoids shown at 30% probability level; selected bond distances: Ir-P(1) = 2.2179(10), Ir-P(2) = 2.2620(10), P(1)-O(1) = 1.625(3), P(2)-O(2) = 1.620(3), Ir-S(1) = 2.4458(10), Ir-Cl(1) = 2.4513(10), Ir-Cl(2) = 2.4436(10), and Ir-C(1) = 2.064(3) Å.

benzylidiphenylphosphine reaction reported in literature.^{47, 48}

On the contrary, upon employment of Na_2CO_3 as the basic catalyst for the *in-situ* coordination of pdpitH and bptzH on the Ir(III) metal atom of $[\text{Ir}(\text{tht})_3\text{Cl}_3]$, we could not isolate any notable quantity of **2**. Instead, we obtained another Ir(III) complex $[\text{Ir}(\text{pdpit})(\text{pppo})(\text{bptz})]$ (**3**) in moderate yields, for which the bright luminescence in solid state can serve as a quick identification. Moreover, both mass spectrometry and ^1H NMR spectrum of **3** showed one less phenyl group on the molecule

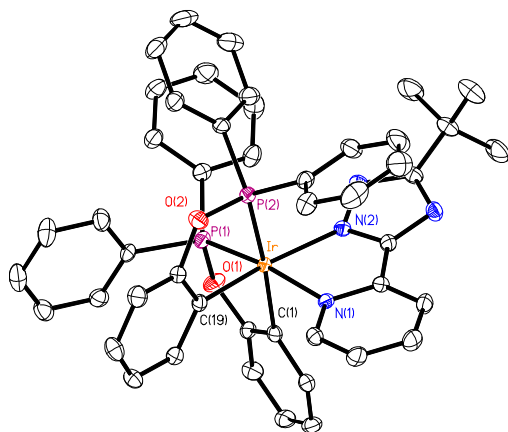


Figure 2. Structural drawing of **2** with ellipsoids shown at 40% probability level; Ir-P(1) = 2.2356(8), Ir-P(2) = 2.2809(8), P(1)-O(1) = 1.634(3), P(2)-O(2) = 1.624(3), Ir-N(1) = 2.144(2), Ir-N(2) = 2.124(3), Ir-C(1) = 2.092(3), and Ir-C(19) = 2.061(3) Å.

versus that of the previously discussed complex **2**. Single crystal X-ray diffraction analyses on all three Ir(III) complexes were next executed for revealing and confirming the true structural identities.

The structural drawings of complexes **1**, **2** and **3** are depicted in Figures 1, 2 and 3 in sequence. As shown in Figure 1, the two chlorides on **1** are residing at the *cis*-disposition, while the unique cyclometalated pdpit chelate is located *trans* to both chlorides, and the remaining axial sites are occupied by the monodentate pdpitH and tht ligand. The Ir-C distance is relatively shorter (ca. 2.064(3) Å), which points to an enhanced covalent bonding character. The respective metallacycle is virtually coplanar, and with the phenyl substituents on the phosphorus atom residing at the opposite direction. Variation of the Ir-Cl and Ir-P distances is somehow relevant to the *trans*-effect discussed earlier. Remarkably, the Ir-P distances of 2.2179(10) and 2.2620(10) Å in **1** (see Figure 1) are shorter than the respective Ir-P distances of 2.2423(8) and 2.3136(7) Å in analogous complex $[\text{Ir}(\text{bdp})(\text{bdpH})(\text{tht})\text{Cl}_2]$, for which the only difference is the phosphine, i.e. pdpitH versus benzylidiphenylphosphine (bdpH).⁴⁸ Since both complexes possess identical geometry, meaning that the shortening of this Ir-P distance in **1** is probably caused by the substitution of methylene in bdpH with an oxo linker in pdpitH, for which the electron withdrawing nature then increases the back π -bonding of the phosphorous donors in **1**. Similarly, the core

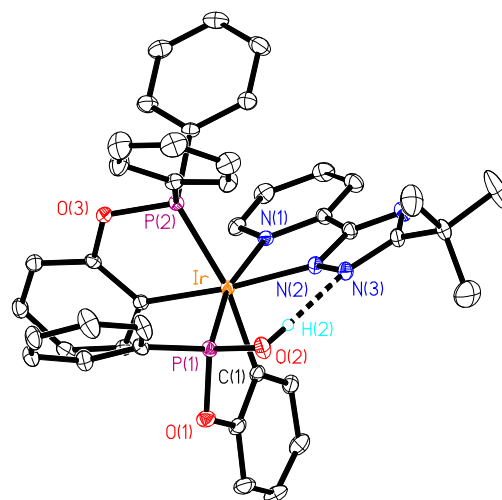


Figure 3. Structural drawing of **3** with ellipsoids shown at 30% probability level; Ir-P(1) = 2.201(1), Ir-P(2) = 2.281(1), Ir-N(1) = 2.146(4), Ir-N(2) = 2.058(4), Ir-C(1) = 2.094(5), Ir-C(13) = 2.076(5), P(1)-O(1) = 1.620(4), P(1)-O(2) = 1.573(4), P(2)-O(3) = 1.614(4), and H(2)⋯N(3) = 1.730 Å.

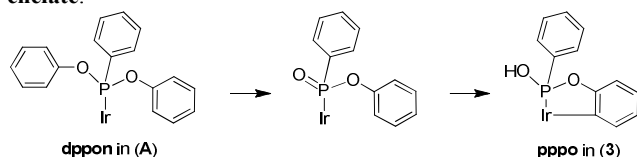
geometry of **2** shown in Figure 2 is also analogous to that of the reported Ir(III) complexes; namely: $[\text{Ir}(\text{bdp})_2(\text{phbtz})]$ ²⁵ and $[\text{Ir}(\text{dpna})_2(\text{iqbtz})]$,²⁶ for which phbtzH, dpnaH and iqbtzH represent 5-(1-phenanthridinyl)-3-*t*-butyl-1,2,4-triazole, 1-(diphenylphosphino)naphthalene and 5-(1-isoquinolyl)-3-*t*-butyl-1,2,4-triazole, respectively. A fair comparison of the metric parameters among these structures cannot be convincingly made due to the structural complexity of the involved phosphine and azolate moieties. Nevertheless, their core geometries are identical, showing one simple criterion in that the all *cis*-coordination mode is detected for the pairs of carbon, nitrogen and phosphorous donor atoms on the inner sphere.

For complex **3**, its structural drawing reveals several distinctive structural features. The first one lies in the formation

of a chelating pppo unit via the loss of a phenyl substituent, which is in agreement with the aforementioned ^1H NMR data. Another important feature is the formation of strong H-bond to the coordinated triazolate with calcd. $\text{H}(2)\cdots\text{N}(3)$ distance of $\sim 1.730 \text{ \AA}$ (Figure 3). In good agreement with this assignment, the ^1H NMR spectrum of a concentrated sample ($1.35 \times 10^{-4} \text{ M}$) in CDCl_3 showed a relative sharp signal at δ 12.42 that can be assigned to this unique proton. However, upon dilution, this signal gradually shifted to the higher field region. At $< 3.4 \times 10^{-5} \text{ M}$, this proton signal shifted to the region of aromatic proton signals and then masked. Such an observation could be attributed to the increase of water content in CDCl_3 and/or greater degree of proton dissociation in the diluted solution.

Coinciding with this H-bonding feature, the $\text{P}(1)\text{-O}(2)$ distance of the unique PO-H (or $\text{P}=\text{O}\text{-H}$) fragment ($1.573(4) \text{ \AA}$) also

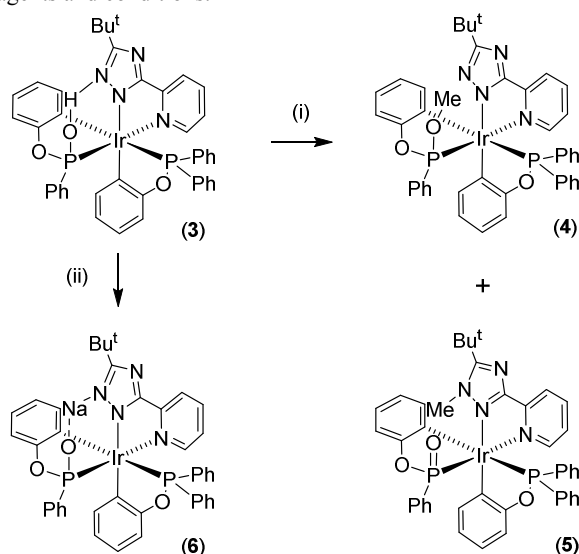
Scheme 2. Hypothetical sequence for formation of pppo chelate.



reduces substantially versus that of other two P-O-Ph fragments ($1.614(4)$ and $1.620(4) \text{ \AA}$) within the molecules. Note that the $\text{P}(1)\text{-O}(2)$ distance is longer than that of the $\text{P}=\text{O}$ double bond in a typical triaryl phosphine oxide fragment ($\sim 1.49 \text{ \AA}$),^{49, 50} indicating the occurrence of PO partial multiple bonding, which fits well to the theoretical bonding model of phenylphosphonite unit. Other notable structural feature includes the shortening of Ir-N(2) separation to the triazolate ($2.058(4) \text{ \AA}$) versus that of the Ir-N(1) distance to the pyridine fragment ($2.146(4) \text{ \AA}$). Apparently, the intermolecular interaction in the crystal packing may also exert certain bond strengthening influence to the triazolate unit.

After confirming the exact structure of **3**, we then

Scheme 3. Reactions associated with the Ir(III) complex **3**; reagents and conditions.^a



^a(i) CH_2N_2 , ether, RT, 4 h, (ii) NaH, RT, 2 h, MeOH. Note: the Na^+ -solvates interaction of **6** was removed for clarity.

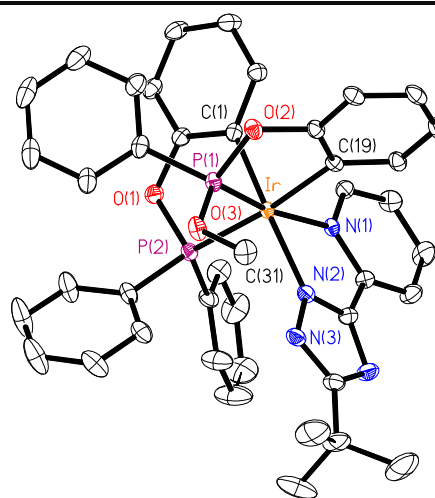


Figure 4. Structural drawing of **4** with ellipsoids shown at 30% probability level; selected bond distances: Ir-C(1) = $2.066(4)$, Ir-C(19) = $2.084(4)$, Ir-N(2) = $2.093(4)$, Ir-N(1) = $2.142(3)$, Ir-P(1) = $2.2137(11)$, Ir-P(2) = $2.2836(10)$, P(1)-O(2) = $1.623(3)$, P(1)-O(3) = $1.585(3)$, P(2)-O(1) = $1.636(3)$, and O(3)-C(31) = $1.457(5) \text{ \AA}$.

investigated the synthetic mechanism in an aim to gain in-depth insight into how this complex was formed in various reaction conditions. First, we conducted a control reaction using **1**, bptzH and 5 equiv. of Na_2CO_3 as the basic promoter, which afforded no compound **3**, but only **2** as the reaction product. This result rules out the possibility that the coordinated pdpitH or cyclometalated pdpit in **1** is the sole source to the coordinated pppo in the formation of **3**. We then performed reaction using **1** and one equiv. of both diphenyl phenylphosphonite (dppon) and bptzH in the presence of excess Na_2CO_3 , which then afforded a small amount of **3** (18%) versus that obtained from its original synthesis (40%, *vide supra*). This result then pinpoints to the possible formation of certain dppon in the original reaction. After then, it reacts with the metal reagent $[\text{IrCl}_3(\text{tht})_3]$ to afford a

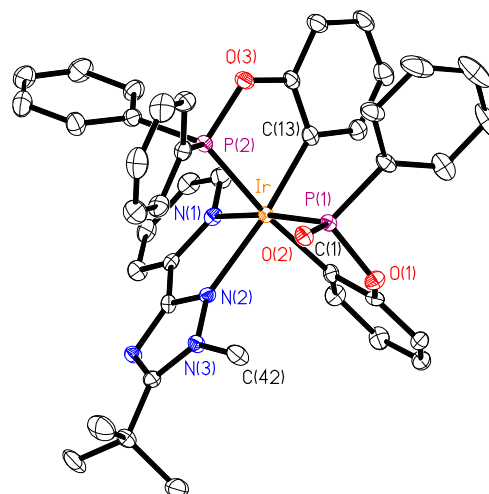


Figure 5. Structural drawing of **5** with ellipsoids shown at 30% probability level; selected bond distances: Ir-C(1) = $2.084(4)$, Ir-C(13) = $2.040(5)$, Ir-N(2) = $2.164(4)$, Ir-N(1) = $2.180(4)$, Ir-P(1) = $2.2613(11)$, Ir-P(2) = $2.2896(12)$, P(1)-O(1) = $1.659(3)$, P(1)-O(2) = $1.492(3)$, P(2)-O(3) = $1.632(3)$, and N(3)-C(42) = $1.464(5) \text{ \AA}$.

possible intermediate (A) (see: Scheme 2). Conversion from coordinated dppon in A to the observed pppo chelate in 3 therefore may follow a hypothetical transformation sequence, which is somewhat relevant to the Arbuzov rearrangement known to the phosphorous chemistry.^{51, 52} The intermediate may involve coordinated P(O)Ph(OPh) fragment, for which the closely related phosphoryl P(O)Ph₂ unit has been obtained from direct oxidation of coordinated PPh₂H with hydrogen peroxide.⁵³ Nevertheless, the overall transformation still remains elusive and pending further proof, as we neither found any precedence for the similar Arbuzov rearrangement in a transition-metal containing system, nor understood which of the reaction (i.e. Arbuzov reaction or cyclometalation) was taking place first. To our experiences, we are confident that the putative dppon must be *in-situ* generated during the treatment of pdpitH with the mixed reagents of [IrCl₃(tht)₃], bptzH and Na₂CO₃ at elevated temperature, because the employed pdpitH is free of phosphonite in all studies, as indicated by both ¹H and ³¹P NMR studies.

Moreover, we also attempted two additional reactions so that the chemical properties of 3 can be assured. The first one involved the reaction with diazomethane etherate at room temperature. As a result, we obtained two methylation products (4) and (5) in 57% and 29%, which respectively showed a ¹H

methyl fragment caused by insertion of the diazomethane (Scheme 3).

For further identification, we then executed the single crystal X-ray studies and the corresponding structural drawings are depicted in Figures 4 and 5. As can be seen, the introduced methyl group is either associated with the oxygen atom of pppo fragment in 4 or the uncoordinated nitrogen atom of bptz fragment in 5, respectively. This result unambiguously confirmed the diazomethane insertion at two difference sites. In comparison to the P-O distance of 3 (1.570(3) Å), the P(1)-O(3) bond in 4 increases to 1.585(3) Å, while the P(1)-O(2) bond in 5 reduced significantly in length to 1.492(3) Å, making the latter as the shortest extreme for the P=O double bond observed in this class of complexes. The similarity in P-O distance between 3 and 4 reaffirms that the P-O-H tautomer is dominated in the solid state for 3. Likewise, as elaborated in the following sections, this assignment also holds true in solution. Nevertheless, it is of great fundamental importance to examine if the proton transfer tautomerism takes place from P-O-H...N (in triazolate moiety) to P=O...H-N isomers in both ground and excited states (vide infra).

In parallel to the diazomethane insertion, which is common to the organic compounds with acidic proton, we also observed a facile deprotonation of 3 upon treatment of NaH in THF at RT. Its progression can be easily monitored by the vigorous evolution of H₂ gas. After filtered off the excess of NaH, crystallization from a mixture of CH₂Cl₂ and methanol afforded pale green crystalline solids of (6) in high yields. Its ¹H and ³¹P NMR spectral patterns are similar to that of 3, showing the first indication for the deprotonation reaction. Moreover, the single crystal X-ray diffraction study showed that this complex exists as a dinuclear dimer that is linked by a four-coordinated sodium cation, each is linked to two methanol solvates related by crystallographical symmetry operation. The structural drawing of one monomeric structure is unveiled in Figure 6 for scrutiny. Except for the coordinative motifs around the sodium cation, the associated metric parameters showed no visible difference from those of parent complex 3, confirming their intimate connection between parent and deprotonated forms.

Photophysical properties.

The photophysical properties of these Ir(III) complexes can be systematically tuned according to the nature of chelate and the associated inter-ligand interaction. Figure 7 displays the absorption and emission spectra of all titled complexes 2 – 6 recorded in degassed CH₂Cl₂ at RT, while pertinent numerical data are summarized in Table 1. In general, all complexes 2 – 6 exhibit allowed absorption bands in the UV region of 275 ~ 284 nm, for which the ε values at the peak wavelength are measured

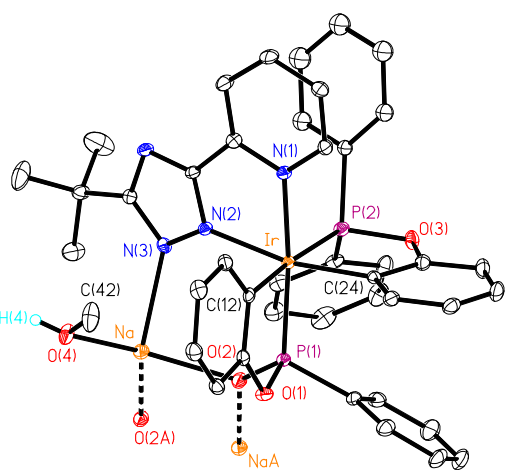


Figure 6. Structural drawing of 6 with ellipsoids shown at 30% probability level; Ir-P(1) = 2.2419(9), Ir-P(2) = 2.2779(10), P(1)-O(1) = 1.652(3), P(1)-O(2) = 1.517(2), P(2)-O(3) = 1.627(3), Ir-N(1) = 2.156(3), Ir-N(2) = 2.124(3), Ir-C(12) = 2.079(4), Ir-C(24) = 2.058(3), Na-O(2) = 2.273(3), Na-O(2A) = 2.292(3), Na-O(4) = 2.346(3), and Na-N(3) = 2.425(3) Å.

NMR signal at δ 4.01 (d, $J_{PH} = 12.0$ Hz, 3H) and δ 5.09 (s, 3H). The integrated signal intensity confirmed their true identity as the

Table 1. Selected photophysical properties of Ir(III) complexes in degassed CH₂Cl₂ solution at RT.

	abs. λ_{max} / nm ($\epsilon \times 10^3$ L mol ⁻¹ cm ⁻¹)	em λ_{max} (nm)	Q.Y.	τ_{obs} (μ s)	k_f (s ⁻¹)	k_{nr} (s ⁻¹)
2	277 (15.7), 360 (3.3)	458, 478, 504	0.01	0.12	8.7×10^4	8.6×10^6
3	276 (15.8), 350 (2.7)	515	0.27	2.32	1.2×10^5	3.1×10^5
4	275 (15.5), 355 (3.6)	460, 475, 505	0.62	21.8	2.8×10^4	1.7×10^4
5	284 (13.8), 348 (1.2)	520	0.11	0.42	2.5×10^5	2.5×10^6
6	283 (16.6), 350 (2.6)	473	0.86	6.72	1.3×10^5	2.1×10^4

to be $> 1.4 \times 10^4 \text{ M}^{-1}\text{cm}^{-1}$ and should be characterized as a $\pi\pi^*$ configuration associated with ligand-centered or inter-ligand type of transition. The longer wavelength absorption at $350 \sim 360 \text{ nm}$, except for **5**, as revealed by their relatively lower extinction coefficients ($3 \sim 5 \times 10^3 \text{ M}^{-1}\text{cm}^{-1}$), is assigned to the tail of $\pi\pi^*$ transition overlapping with the metal-to-ligand charge transfer (MLCT) band in the singlet manifold.^{54,55} Time-

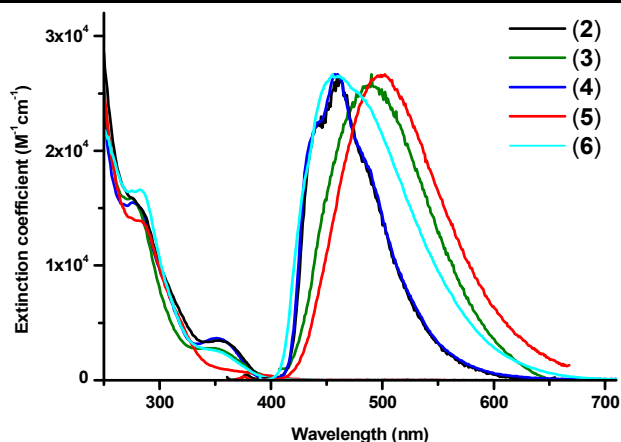


Figure 7. Absorption and luminescence spectra of Ir(III) complexes in degassed CH_2Cl_2 at room temperature.

dependent (TD) DFT calculations were performed to gain insight into the photophysical behavior of all of the titled complexes. Figure 8 depicts the unoccupied and occupied frontier orbitals of **2 – 6** that are mainly involved in the lowest-lying transitions. Description and details of the energy gap of each transition of all complexes are given in Table 2. Careful frontier orbital analyses for **2 – 6** indicate that the lowest lying electronically excited state involves HOMO \rightarrow LUMO transition, in which HOMO is mainly located at Ir(III) metal ion and the phenolic cyclometalate of the phenyl phenylphosphonite moiety. Additionally, HOMO contribution from the triazolate moiety is also found in **2 – 4** and **6** but not in **5**. The methylation at N(3) of triazolate for **5** (see Figure 5) results in the relocation of electron density so that the electronic configuration of the triazolate fragment is expected to be much different from that of **2 – 4** and **6**. For example, from chemistry point of view, the Ir-N(2) linkage for **5** is considered to be a neutral dative bonding instead of an ionic bonding as observed for the rest of Ir(III) complexes. On the other hand, the calculation also clearly shows that LUMO for all titled complexes is mainly located at the entire pyridyl triazolate moieties.⁵⁶ As a result, the electronic transition property for **5** is expected to be significantly different from that of **2 – 4** and **6**. This prediction well matches the absorption spectra, for which the lowest lying

absorption bands for **2 – 4** and **6** in CH_2Cl_2 resemble each other in terms of spectral profile and peak wavelength. In stark contrast, however, complex **5** reveals a much diffusive, red-shifted absorption feature. Comparing isomers **4** and **5**, **4** exhibits an $S_0 \rightarrow S_1$ absorption peak at 355 nm , while **5** reveals a shoulder around 380 nm tailing down to $\sim 420 \text{ nm}$ (see Figure 7 and Table 2). This is also supported by the computation result, giving much different $S_0 \rightarrow S_1$ transition at 365 nm and 420 nm for **4** and **5**, respectively, which is well correlated with the absorption spectra. Also supportive is the calculated oscillator strength, for which the value of 0.0289 in **4** is much larger than that of **5** (0.0025), qualitatively predicting the same trend as the molar extinction coefficient being $3.6 \times 10^3 \text{ M}^{-1}\text{cm}^{-1}$ and $1.2 \times 10^3 \text{ M}^{-1}\text{cm}^{-1}$ for **4** and **5**, respectively. The discrepancy between the absorption and calculation in terms of intensity ratio for **4** versus **5** is mainly due to the negligence of the vibronic coupling, i.e., the Franck Condon factor in our computational approach. The results not only manifest the influence of methylated triazolate moiety to the frontier orbitals in **5** (vide supra) but also indicate that the TDDFT calculation is well justified for interpreting the photophysical properties of the titled Ir(III) complexes. It is noticeable that the complexes **2** and **4** display a slightly higher absorptivity for the $S_0 \rightarrow S_1$ band versus that of complexes **3** and **6**; the latter reveal unique inter-ligand (either H^+ , i.e. H-bond, or Na^+) cation-to-triazolate bonding interaction, resulting in the reduction of $\pi\pi^*$ transition dipole moment.

As for the emission spectra, the significant variation of intensity between aerated and degassed solution, i.e. the great influence of O_2 quenching, together with the $< 10^6 \text{ s}^{-1}$ of the

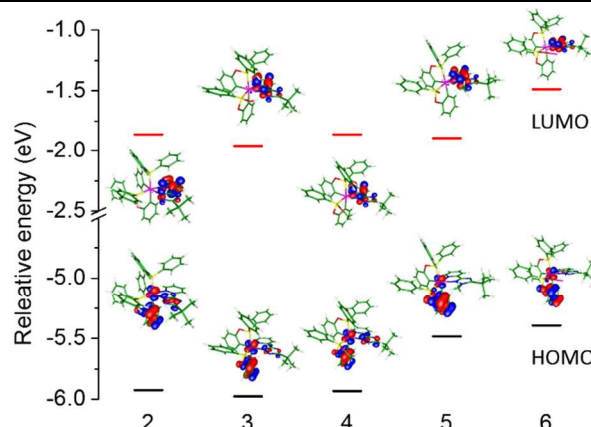


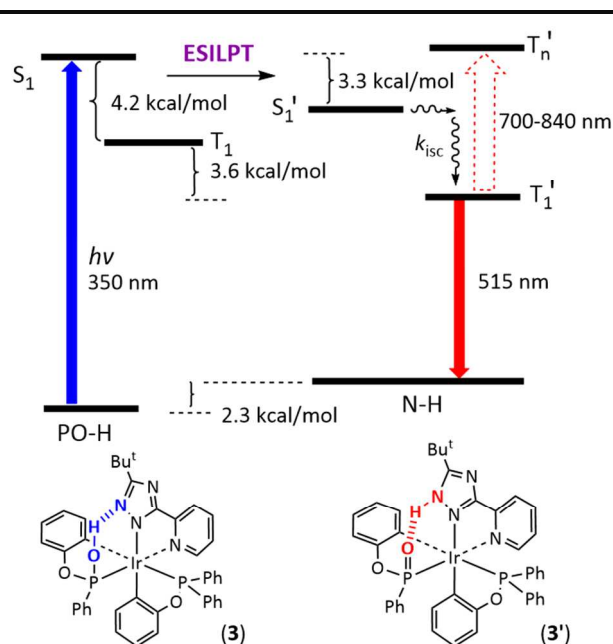
Figure 8. Frontier orbitals involved in the lowest-lying transition for complexes **2 – 6** in CH_2Cl_2 . Note that the calculation for **3** is based on PO-H isomer in order to simulate the absorption properties.

Table 2. Calculated vertical excitation S_1 energy and the involved frontier orbitals.

Complex	State	(nm)	f	Assignments	MLCT (%)
2	S_1	366.1	0.0267	HOMO \rightarrow LUMO (98%)	26.49
3 (w/ PO-H)	S_1	370.5	0.0251	HOMO \rightarrow LUMO (98%)	22.08
	S_1	410.4	0.0161	HOMO \rightarrow LUMO (97%)	18.08
4	S_1	365.2	0.0289	HOMO \rightarrow LUMO (98%)	26.14
5	S_1	420.4	0.0025	HOMO \rightarrow LUMO (98%)	12.81
6	S_1	381.4	0.0083	HOMO \rightarrow LUMO (98%)	18.59

radiative decay rate constant, for all titled complexes (see Table 1) ensures that the emission originates from the triplet manifold, i.e. the phosphorescence. It is noteworthy that all these emission profiles and the associated relaxation dynamics in solution are independent of concentrations employed, eliminating the possible inter-molecular $\pi\pi$ stacking interaction of the titled complexes in both ground and excited states. Interestingly, despite that **3** has similar transition character and absorption spectral feature with **2**, **4** and **6**, distinct emission spectrum for **3** is observed. Complexes **2**, **4** and **6** all exhibit similar phosphorescent spectra maximized around 473 ~ 478 nm with notable vibronic progression. In sharp contrast, **3** reveals much red-shifted and structureless emission maximized at 515 nm. More importantly, **3** exhibits nearly identical phosphorescence spectrum with that of **5** in terms of peak profile and position (Figure 7). Unambiguously, complex **5** possesses a methylated triazolate moiety. The result thus leads us to propose the possibility of excited-state inter-ligand proton transfer (ESILPT) from the PO-H to N-H isomer via the existing H-bond between O-H of phosphonite fragment and the non-coordinative N(2) atom of the triazolate ligand (see Scheme 4). Moreover, the frontier orbital analysis provided certain clue for the tendency of ESILPT. Upon $S_0 \rightarrow S_1$ excitation the electron density shifts from the phenyl cyclometalate of the phosphonite moiety (HOMO) to the pyridyl triazolate moiety (LUMO), shown in Figure 8. In other words, the PO-H proton becomes more acidic while the triazolate N(2) nitrogen tends to be more basic in the S_1 state, providing the driving force for ESILPT.

We then carefully examined the feasibility in view of thermodynamics for this proposed mechanism from the computational approach. We first calculated the relative energy difference between PO-H and N-H isomers in the ground state (in



Scheme 4. The proposed excited-state inter-ligand proton transfer (ESILPT) for **3** from the PO-H to the N-H tautomer (in CH_2Cl_2). The differences in energy between PO-H and N-H in ground and excited states are obtained from the computational approach (see Table 2 for detail).

CH_2Cl_2). Upon full geometry optimization for both isomers, the result indicates that PO-H is more stable than N-H by 2.35 kcal/mol (see experimental section). Note that this calculated result is independent of the selected solvents, being 2.40 and 2.33 kcal/mol calculated in cyclohexane and acetonitrile, respectively. Therefore the PO-H isomer for **3** should be the predominant species in solution, while the population of N-H isomer is < 2% in the ground state. This prediction is consistent with the conclusion made from the absorption spectrum as well as the PO-H structure verified by single crystal X-ray analysis (vide supra). Further calculation was then performed by vertically exciting both PO-H and N-H isomers, resulting in an $S_0 \rightarrow S_1$ transition in terms of wavelength of 365 and 420 nm, respectively (see Table 2). Subsequently, the geometry of the lowest lying excited state for PO-H and N-H isomers in both singlet and triplet states was fully optimized. As a result, all corresponding relative energetics

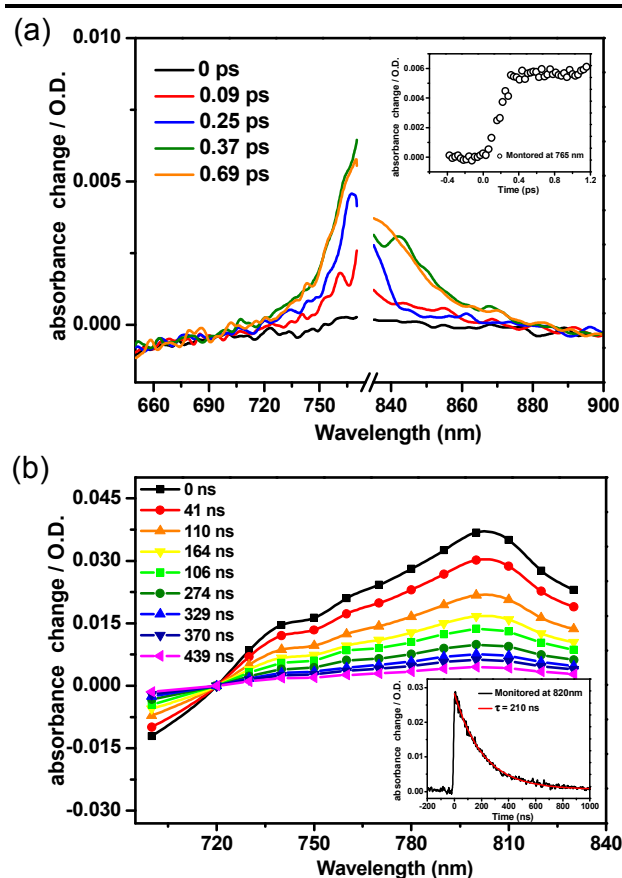


Figure 9. (a) Femtosecond transient absorption experiment of complex **3** in CH_2Cl_2 . The insert showed the pump-probe delay time with $\lambda_{\text{ex}} = 400$ nm. Note that the transient absorption at ~800 nm region is filtered out due to the unavoidable leakage of 800 nm laser used for the white-light generation. (b) The nanosecond transient absorption experiment of complex **3** in CH_2Cl_2 . The insert showed the pump-probe delay time with $\lambda_{\text{ex}} = 355$ nm and monitored at 820 nm. Both femtosecond and nanosecond transient absorption measurements are performed in the aerated CH_2Cl_2 .

and energy gaps are indicated in Scheme 4. The result clearly shows that PO-H \rightarrow N-H ESILPT is thermodynamically allowed by 3.3 and 3.6 kcal/mol, respectively, in singlet and triplet manifolds. We will discuss these two competitive pathways in the later section.

From the dynamics point of view, the rate of ESILPT should be fast due to the light weighted proton so that tunnelling may take place along the potential energy surface associated with H-bond. Experimentally, we have made attempts to measure the rise time of the 515 nm phosphorescence by time correlated single photon counting (TCSPC) technique; the result monitored at 515 nm shows a fast rise component, which is beyond the system response limit of 50 ps. We then further probed the relaxation dynamics by using femtosecond transient absorption technique. Upon 400 nm excitation (~100 fs pulse duration, 1 kHz repetition rate), the result shows a transient absorption band maximized approximately at ~760-840 nm (Figure 9a). The actual position unfortunately is obscure due to the use of interference filter to eliminate the fundamental pulse (800 nm) for the white light generation. Despite the unsolved peak wavelength, the spectral feature of femtosecond transient absorption band resembles that acquired by nanosecond transient absorption maximized at ~805 nm (see Figure 9b).

The rise time of the transient absorption monitored at e.g., 765 nm (see inset of Figure 9a) is fitted to be beyond the system response limit of 220 fs, while the population decay is exceedingly long, being virtually constant throughout the measurement period of 100 ps. As shown in inset of Figure 9, the population decay time of the transient absorption can be further fitted by the nanosecond transient absorption data, which is

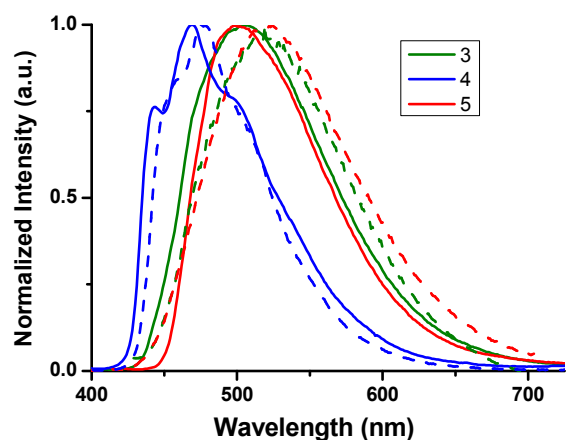


Figure 10. Photoluminescence spectra of Ir(III) complexes **3** ~ **5** in solid powder (solid lines) and in degassed CH_2Cl_2 at RT (dashed lines).

calculated to be 210 ns in CH_2Cl_2 (see inset of Figure 9b). This value is identical with the decay time of phosphorescence (~210 ns) under the same experimental condition. The result unambiguously concludes that the ~720-840 nm transient absorption band originates from the $T_1 \rightarrow T_n$ absorption, which is most probably associated with the proton transfer tautomer species in the triplet manifold.

Further pursuit regarding whether ESILPT takes place in the singlet or in the triplet manifold is also of great fundamental interest. Documented in numerous reports, ESIPT commonly takes place in the singlet manifold with ultrafast ($\ll 1$ ps) reaction dynamics.^{1,2} In other words, ESIPT is normally associated with negligibly small barrier or even barrierless so that the reaction takes place either in a ballistic type or in a coherent motion association involving certain vibrational modes associated with H bond.^{1,2} It is thus reasonable to expect that **3** undergoes

ultrafast ESILPT in the singlet manifold, followed by the fast $S_1' \rightarrow T_1'$ intersystem crossing in the N-H proton transfer isomer (see Scheme 4). Additionally, intramolecular proton transfer in the triplet manifold was rarely experimentally identified. The acidity of the proton donor in the triplet manifold is usually decreased,⁵² resulting in substantial barrier that prohibits ESIPT. Similar PO-H \rightarrow N-H ESILPT occurs for **3** in solid state, as evidenced by the nearly identical emission spectrum between **3** and **5**, in terms of spectral profile and peak wavelength, as opposed to the drastic difference in spectrum between **3** and **4** shown in Figure 10. The spectra of **3** in solid state and solution are very similar; the slight red shift in solution is probably due to the flexible solvent relaxation process.

The rest complexes **2**, **4** and **6** possess P-O-M bonding character (M could be phenyl, methyl or even Na^+ in **6**), such that the triazolote moiety remains intact without protonation (cf. **3**, N-

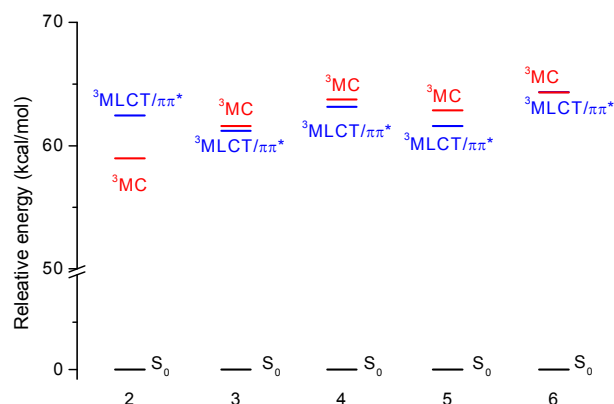


Figure 11. Energy diagram of complexes **2** ~ **6** depicted in terms of ^3MC and $^3\text{MLCT}/\pi\pi^*$ excited states, in which all states were obtained from unrestricted optimization, the ^3MC dd excited state is also refined by the same method, but the initial structure is from a highly distorted molecular geometry. Note that for complex **3** the N-H isomer is applied in this approach to simulate the emission properties.

H isomer) or alkylation (cf. **5**, with N-Me). Therefore, their spectral feature is expected to be similar. For example, the spectral profile and the vibronic coupling pattern of complexes **2** and **4** seem virtually identical to each other as well as to other Ir(III) complexes decorated with the 2-pyridyl triazolote chelate,^{23,26,57} reaffirming that the triazolote chelate plays key role in emission spectral characteristic.

We then discuss the general trend of the decay dynamics and its correlation with emission quantum yield among the titled complexes. The P-Ir dative bonding in is able to further destabilize the metal-centered dd excited states, thereby suppressing nonradiative decay pathways, if the dd excited state is the major quenching process. Standing on this point, the electron-donating strength of phosphorous donors should be in the order of $\text{P}(\text{O}^-\text{Ph})\text{Ph}(\text{X})$ (**3**: $\text{X} = -\text{OH}$, **4**: $\text{X} = -\text{OMe}$, **5**: $\text{X} = =\text{O}$) $>$ $\text{P}(\text{O}^-\text{Ph})\text{Ph}_2$ (**2**). Therefore, the dd excited state should be least destabilized in **2**. This is supported by the computational approach, in which the geometry optimization along the triplet potential energy surface (PES) is performed and the relatively energy gap between $^3\text{MLCT}/\pi\pi^*$ and ^3MC dd states for complexes **2** – **6** is calculated and shown in Figure 11. For complex **3**, the N-H proton-transfer isomer is applied in this

approach due to its contribution to the emission. The $^3\text{MC dd}$ excited state possesses a repulsive PES, which in theory will touch the ground-state PES, resulting in the dominant radiationless deactivation process if it is lower in energy than that of the emissive $^3\text{MLCT}/\pi\pi^*$ state. As expected, the $^3\text{MC dd}$ state for **2** is substantially lower in energy than that of the proximal $^3\text{MLCT}/\pi\pi^*$ state (see Figure 11). The result rationalizes the lowest emission quantum yield ($\Phi = 0.01$), shortest emission lifetime ($\tau_{\text{obs}} = 0.12 \mu\text{s}$) and highest nonradiative decay rate constant k_{nr} of $8.6 \times 10^6 \text{ s}^{-1}$ for **2** in solution. The rest of Ir(III) complexes **3** – **6** show $^3\text{MLCT}/\pi\pi^*$ to be the lowest emissive state and hence the high phosphorescence yield of > 0.1 (see Table 1).

Conclusion

We report the new insight into the chemistry of a series of Ir(III) complexes **1** – **6** bearing pyridyl triazolate and phenyl phenylphosphonite cyclometalate. The reaction reveals distinct reaction pathway as a function of catalyst basicity, cf. NaOAc and Na_2CO_3 . Using **3** as a representative, its formation incorporates temporal formation of diphenyl phenylphosphonite, followed by elimination of a phenyl group to give phenyl phenylphosphonite and concomitant cyclometalation and bptz coordination. For **3**, the existence of either PO-H or N-H bonding isomer or both is of fundamental interest and has been probed by comparative photophysical properties between **3** and its methylated PO-Me (**4**) and N-Me (**5**) derivatives. As a result, the PO-H isomer is concluded to be the dominant species in both solid crystal and solution. Remarkably, despite the existence of PO-H isomer, its N-Me (**5**)-like emission properties lead us to conclude the occurrence of ES IPT, resulting in an N-H isomer and showing relevant emission. The observation of H-bonding tautomerism, especially the proton transfer from inter-ligands in the framework of transition metal complex is apparently unprecedented, which adds a new chapter to those reported for the ES IPT process mostly taking place in the fluorescent organic molecules. The results should thus attract a broad spectrum of interest from both fundamental and application aspect in harnessing the luminescence and perhaps photo-catalytic properties via formation of H-bonding.

ASSOCIATED CONTENT

X-ray crystallographic data file (CIF) of all studied Ir(III) metal complexes **1** – **6**. This material is available free of charge via the internet at <http://www.rsc.org>

AUTHOR INFORMATION

Corresponding Authors

ychi@mx.nthu.edu.tw; chop@ntu.edu.tw

Notes

The authors declare no competing financial interest.

Acknowledgment

We thank the Ministry of Science and Technology of Taiwan (MOST) for financial supports.

REFERENCES

- C.-C. Hsieh, C.-M. Jiang and P.-T. Chou, *Acc. Chem. Res.*, 2010, **43**, 1364.
- A. P. Demchenko, K.-C. Tang and P.-T. Chou, *Chem. Soc. Rev.*, 2013, **42**, 1379.
- C. A. Wraight, *Biochim. Biophys. Acta, Bioenerg.*, 2006, **1757**, 886.
- P. T. Chou, M. L. Martinez, W. C. Cooper, S. T. Collins, D. P. McMorrow and M. Kasha, *J. Phys. Chem.*, 1992, **96**, 5203.
- P.-T. Chou, C.-Y. Wei, C.-P. Chang and M.-S. Kuo, *J. Phys. Chem.*, 1995, **99**, 11994.
- P.-T. Chou, W.-S. Yu, Y.-C. Chen, C.-Y. Wei and S. S. Martinez, *J. Am. Chem. Soc.*, 1998, **120**, 12927.
- P.-T. Chou, G.-R. Wu, C.-Y. Wei, M.-Y. Shiao and Y.-I. Liu, *J. Phys. Chem. A*, 2000, **104**, 8863.
- P.-T. Chou, J.-H. Liao, C.-Y. Wei, C.-Y. Yang, W.-S. Yu and Y.-H. Chou, *J. Am. Chem. Soc.*, 2000, **122**, 986.
- W.-T. Hsieh, C.-C. Hsieh, C.-H. Lai, Y.-M. Cheng, M.-L. Ho, K. K. Wang, G.-H. Lee and P.-T. Chou, *ChemPhysChem*, 2008, **9**, 293.
- W.-P. Hu, J.-L. Chen, C.-C. Hsieh and P.-T. Chou, *Chem. Phys. Lett.*, 2010, **485**, 226.
- P.-T. Chou, W.-S. Yu, C.-Y. Wei, Y.-M. Cheng and C.-Y. Yang, *J. Am. Chem. Soc.*, 2001, **123**, 3599.
- A. P. Demchenko, *Biochim. Biophys. Acta*, 1994, **1209**, 149.
- A. Douhal, S. K. Kim and A. H. Zewail, *Nature*, 1995, **378**, 260.
- M. Chachisvilis, T. Fiebig, A. Douhal and A. H. Zewail, *J. Phys. Chem. A*, 1998, **102**, 669.
- O.-H. Kwon and A. H. Zewail, *Proc. Natl. Acad. Sci. U. S. A.*, 2007, **104**, 8703.
- H. Lim, S.-Y. Park and D.-J. Jang, *J. Phys. Chem. A*, 2010, **114**, 11432.
- S.-Y. Park, Y.-S. Lee and D.-J. Jang, *Phys. Chem. Chem. Phys.*, 2011, **13**, 3730.
- Y.-C. Chiu, J.-Y. Hung, Y. Chi, C.-C. Chen, C.-H. Chang, C.-C. Wu, Y.-M. Cheng, Y.-C. Yu, G.-H. Lee and P.-T. Chou, *Adv. Mater.*, 2009, **21**, 2221.
- C.-H. Lin, Y.-Y. Chang, J.-Y. Hung, C.-Y. Lin, Y. Chi, M.-W. Chung, C.-L. Lin, P.-T. Chou, G.-H. Lee, C.-H. Chang and W.-C. Lin, *Angew. Chem. Int. Ed.*, 2011, **50**, 3182.
- Y.-Y. Chang, J.-Y. Hung, Y. Chi, J.-P. Chyn, M.-W. Chung, C.-L. Lin, P.-T. Chou, G.-H. Lee, C.-H. Chang and W.-C. Lin, *Inorg. Chem.*, 2011, **50**, 5075.
- V. Sivasubramaniam, F. Brodkorb, S. Hanning, H. P. Loebl, V. van Elsbergen, H. Boerner, U. Scherf and M. Kreyenschmidt, *J. Fluorine Chem.*, 2009, **130**, 640.
- F. So and D. Kondakov, *Adv. Mater.*, 2010, **22**, 3762.
- Y. Chi, B. Tong and P.-T. Chou, *Coord. Chem. Rev.*, 2014, DOI: 10.1016/j.ccr.2014.08.012.
- C.-H. Lin, C.-Y. Lin, J.-Y. Hung, Y.-Y. Chang, Y. Chi, M.-W. Chung, Y.-C. Chang, C. Liu, H.-A. Pan, G.-H. Lee and P.-T. Chou, *Inorg. Chem.*, 2012, **51**, 1785.
- C.-H. Lin, Y. Chi, M.-W. Chung, Y.-J. Chen, K.-W. Wang, G.-H. Lee, P.-T. Chou, W.-Y. Hung and H.-C. Chiu, *Dalton Trans.*, 2011, **40**, 1132.
- J.-Y. Hung, C.-H. Lin, Y. Chi, M.-W. Chung, Y.-J. Chen, G.-H. Lee, P.-T. Chou, C.-C. Chen and C.-C. Wu, *J. Mater. Chem.*, 2010, **20**, 7682.
- J.-Y. Hung, Y. Chi, I.-H. Pai, Y.-M. Cheng, Y.-C. Yu, G.-H. Lee, P.-T. Chou, K.-T. Wong, C.-C. Chen and C.-C. Wu, *Dalton Trans.*, 2009, 6472.
- Y.-C. Chiu, C.-H. Lin, J.-Y. Hung, Y. Chi, Y.-M. Cheng, K.-W. Wang, M.-W. Chung, G.-H. Lee and P.-T. Chou, *Inorg. Chem.*, 2009, **48**, 8164.

29. J. E. Kwon and S. Y. Park, *Adv. Mater.*, 2011, **23**, 3615.
30. J. Wu, W. Liu, J. Ge, H. Zhang and P. Wang, *Chem. Soc. Rev.*, 2011, **40**, 3483.
31. K. Kuroda, Y. Maruyama, Y. Hayashi and T. Mukaiyama, *Bull. Chem. Soc. Jpn.*, 2009, **82**, 381.
32. M. Hudlicky, *J. Org. Chem.*, 1980, **45**, 5377.
33. G. M. Sheldrick, *Acta Cryst.*, 2008, **A64**, 112.
34. C.-C. Hsieh, P.-T. Chou, C.-W. Shih, W.-T. Chuang, M.-W. Chung, J. Lee and T. Joo, *J. Am. Chem. Soc.*, 2011, **133**, 2932.
35. C. Lee, W. Yang and R. G. Parr, *Phys. Rev. B*, 1988, **37**, 785.
36. A. D. Becke, *J. Chem. Phys.*, 1993, **98**, 5648.
37. P. J. Hay and W. R. Wadt, *J. Chem. Phys.*, 1985, **82**, 284.
38. P. J. Hay and W. R. Wadt, *J. Chem. Phys.*, 1985, **82**, 299.
39. P. C. Hariharan and J. A. Pople, *Mol. Phys.*, 1974, **27**, 209.
40. C. Jamorski, M. E. Casida and D. R. Salahub, *J. Chem. Phys.*, 1996, **104**, 5134.
41. M. Petersilka, U. J. Gossmann and E. K. U. Gross, *Phys. Rev. Lett.*, 1996, **76**, 1212.
42. R. Bauernschmitt, R. Ahlrichs, F. H. Hennrich and M. M. Kappes, *J. Am. Chem. Soc.*, 1998, **120**, 5052.
43. M. E. Casida, C. Jamorski, K. C. Casida and D. R. Salahub, *J. Chem. Phys.*, 1998, **108**, 4439.
44. R. E. Stratmann, G. E. Scuseria and M. J. Frisch, *J. Chem. Phys.*, 1998, **109**, 8218.
45. E. Cancès, B. Mennucci and J. Tomasi, *J. Chem. Phys.*, 1997, **107**, 3032.
46. M. J. Frisch, G. W. Trucks, H. B. Schlegel, G. E. Scuseria, M. A. Robb, J. R. Cheeseman, G. Scalmani, V. Barone, B. Mennucci, G. A. Petersson, H. Nakatsuji, M. Caricato, X. Li, H. P. Hratchian, A. F. Izmaylov, J. Bloino, G. Zheng, J. L. Sonnenberg, M. Hada, M. Ehara, K. Toyota, R. Fukuda, J. Hasegawa, M. Ishida, T. Nakajima, Y. Honda, O. Kitao, H. Nakai, T. Vreven, J. A. Montgomery, J. E. Peralta, F. Ogliaro, M. Bearpark, J. J. Heyd, E. Brothers, K. N. Kudin, V. N. Staroverov, R. Kobayashi, J. Normand, K. Raghavachari, A. Rendell, J. C. Burant, S. S. Iyengar, J. Tomasi, M. Cossi, N. Rega, J. M. Millam, M. Klene, J. E. Knox, J. B. Cross, V. Bakken, C. Adamo, J. Jaramillo, R. Gomperts, R. E. Stratmann, O. Yazyev, A. J. Austin, R. Cammi, C. Pomelli, J. W. Ochterski, R. L. Martin, K. Morokuma, V. G. Zakrzewski, G. A. Voth, P. Salvador, J. J. Dannenberg, S. Dapprich, A. D. Daniels, Farkas, J. B. Foresman, J. V. Ortiz, J. Cioslowski and D. J. Fox, *Gaussian 09, Revision A.1; Gaussian Inc.*, 2009, Wallingford.
47. B.-S. Du, C.-H. Lin, Y. Chi, J.-Y. Hung, M.-W. Chung, T.-Y. Lin, G.-H. Lee, K.-T. Wong, P.-T. Chou, W.-Y. Hung and H.-C. Chiu, *Inorg. Chem.*, 2010, **49**, 8713.
48. C.-H. Lin, Y.-C. Chiu, Y. Chi, Y.-T. Tao, L.-S. Liao, M.-R. Tseng and G.-H. Lee, *Organometallics*, 2012, **31**, 4349.
49. D. Kim, S. Salman, V. Coropceanu, E. Salomon, A. B. Padmaperuma, L. S. Sapochak, A. Kahn and J.-L. Bredas, *Chem. Mater.*, 2010, **22**, 247.
50. C.-H. Lin, C.-W. Hsu, J.-L. Liao, Y.-M. Cheng, Y. Chi, T.-Y. Lin, M.-W. Chung, P.-T. Chou, G.-H. Lee, C.-H. Chang, C.-Y. Shih and C.-L. Ho, *J. Mater. Chem.*, 2012, **22**, 10684.
51. W. Dabkowski, A. Ozarek, S. Olejniczak, M. Cypryk, J. Chojnowski and J. Michalski, *Chem. Eur. J.*, 2009, **15**, 1747.
52. P.-Y. Renard, P. Vayron and C. Mioskowski, *Org. Lett.*, 2003, **5**, 1661.
53. E. Lebon, R. Sylvain, R. E. Piau, C. Lanthony, J. Pilmé, P. Sutra, M. Boggio-Pasqua, J.-L. Heully, F. Alary, A. Juris and A. Igau, *Inorg. Chem.*, 2014, **53**, 1946.
54. Y.-S. Yeh, Y.-M. Cheng, Yi-Ming P.-T. Chou, G.-H. Lee, C.-H. Yang, Y. Chi, C.-F. Shu and C.-H. Wang, *ChemPhysChem*, 2006, **7**, 2294.
55. S.-Y. Chang, J. Kavitha, J.-Y. Hung, Y. Chi, Y.-M. Cheng, E. Y. Li, P.-T. Chou, G.-H. Lee and A. J. Carty, *Inorg. Chem.*, 2007, **46**, 7064.
56. F.-C. Hsu, Y.-L. Tung, Y. Chi, C.-C. Hsu, Y.-M. Cheng, M.-L. Ho, P.-T. Chou, S.-M. Peng and A. J. Carty, *Inorg. Chem.*, 2006, **45**, 10188.
57. C.-H. Chang, C.-L. Ho, Y.-S. Chang, I.-C. Lien, C.-H. Lin, Y.-W. Yang, J.-L. Liao and Y. Chi, *J. Mater. Chem. C*, 2013, **1**, 2639.

